BEHAVIOR OF CONCRETE BRIDGE DECKS REINFORCED WITH MMFX STEEL

Hatem Seliem, Gregory Lucier, Sami Rizkalla and Paul Zia
Civil Engineering Department. North Carolina State University, USA
E-mail: sami_rizkalla@ncsu.edu

Introduction

Corrosion of steel reinforcement is considered to be one of the leading causes of deterioration of concrete bridges. This fact has led to the development of numerous technologies such as corrosion-resistant steel that attempt to mitigate this expensive problem. The recent development of high-strength, highly corrosion-resistant steel, commercially known as Micro-composite Multi-Structural Formable (MMFX) steel, is a promising technology. MMFX steel offers its high corrosion resistance without the use of the coating technologies. This characteristic was achieved by proprietary alteration of the steel composition and microstructure. In addition, the control of MMFX steel's morphology of its microstructure has resulted in its higher strength. Use of MMFX steel could lead to potential savings through using less reinforcement ratios due to its higher strength characteristics and longer service life of structures because of its high corrosion resistance. Recently, many state transportation departments have begun to use MMFX steel as a direct replacement for conventional Grade 60 steel in concrete bridge decks. However, despite these field applications, there is insufficient information about the behavior of such concrete bridge decks utilizing MMFX steel as main reinforcement.

This paper evaluates the use of MMFX steel as main flexural reinforcement in concrete bridge decks in light of test results. Assessment of the effect of the arching action on the strength of bridge decks due to the use of this new steel is also presented.

Experimental Program

Specimen Details

The experimental program consisted of testing three full-scale bridge decks with a span-to-depth ratio of 12.5 to evaluate the structural performance of MMFX steel as main flexural reinforcement in comparison to the use of conventional Grade 60 steel. The bridge decks were identical in all aspects except for the type and amount of steel used in each. The bridge decks consisted of two spans and two cantilevers, supported in composite action by three pre-cast post-tensioned concrete girders having cross-sectional dimensions of 24×10 in. (610×254 mm). The overall nominal dimensions of the bridge decks were $21' - 10'' \times 13' - 2'' \times 8\,^5/_8''$ ($6655 \times 4013 \times 220$ mm). The supporting girders were post-tensioned using deformed prestressing bars of 1 in. (25 mm) diameter with ultimate strength of 150 ksi (1034 MPa). Each girder was prestressed by four bars resulting in a total prestressing force of 360 kips (1601 KN) per girder.

The first and third bridge decks were reinforced with MMFX steel, while the second bridge deck was reinforced with conventional Grade 60 steel for comparison purposes. The test matrix is given in Table 1 and the reinforcement details for the three bridge decks are shown in Figure 1. It should be noted that the reinforcement ratio (ρ) is calculated using the total slab thickness. The first and second bridge decks were constructed with the same reinforcement ratio using MMFX and conventional Grade 60 steel, respectively. However, the third bridge deck was reinforced with MMFX steel using only two-third of the reinforcement ratio used for the first deck in an attempt to utilize the higher

Table 1. Bridge decks test matrix.

Bridge Deck	Steel Type	Bottom Reinforcement		Top Reinforcement	
		Transverse	Longitudinal	Transverse	Longitudinal
First	MMFX	#5 @ 6.75" (#16 @ 170) $\rho = 0.54\%$	#5 @ 10" (#16 @ 250) $\rho = 0.36\%$	#5 @ 6.75" (#16 @ 170) $\rho = 0.54\%$	#4 @ 14" (#13 @ 360) $\rho = 0.17\%$
Second	Grade 60	#5 @ 6.75" (#16 @ 170) $\rho = 0.54\%$	#5 @ 10" (#16 @ 250) $\rho = 0.36\%$	#5 @ 6.75" (#16 @ 170) $\rho = 0.54\%$	#4 @ 14" (#13 @ 360) $\rho = 0.17\%$
Third	MMFX	#5 @ 10" (#16 @ 250) $\rho = 0.36\%$	#5 @ 10" (#16 @ 250) $\rho = 0.36\%$	#5 @ 10" (#16 @ 250) $\rho = 0.36\%$	#4 @ 14" (#13 @ 360) $\rho = 0.17\%$

Reinforcement Details of the First and Second Bridge Decks

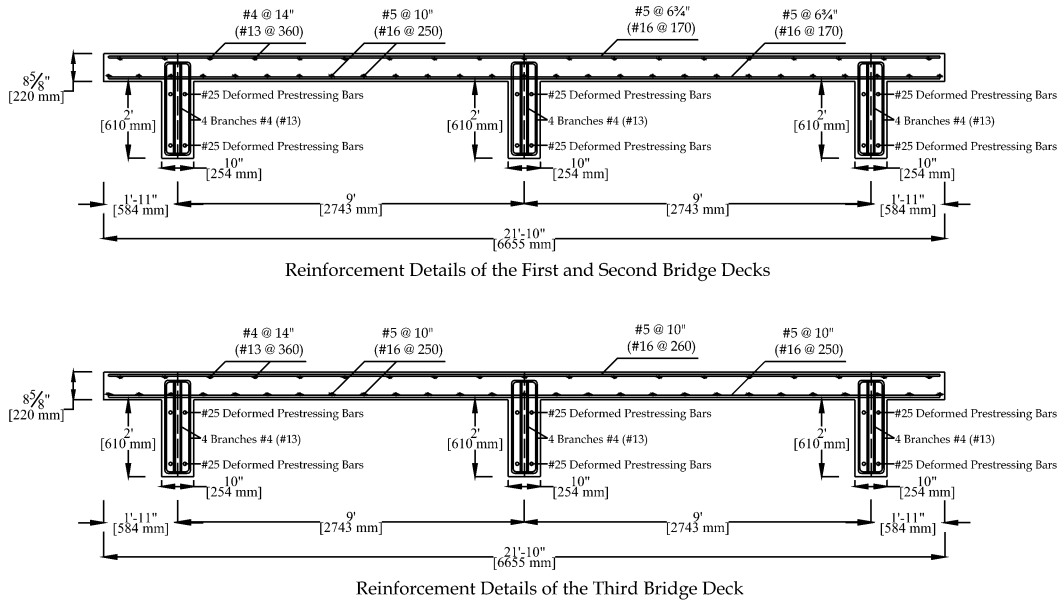Reinforcement Details of the Third Bridge Deck

Fig. 1. Reinforcement details for the three bridge decks.

tensile strength of MMFX steel. It should be noted that the first bridge deck was designed to simulate the same reinforcement ratio of an actual bridge that was built in Johnston County, North Carolina in 2004. The three bridge decks had the same span and thickness of the bridge, and supported by girders designed to have the same torsional stiffness as the actual bridge.

Material Properties

The average concrete compressive strength at the day of testing for the three bridge decks was 7000, 4500, and 5278 psi (48.2, 31, and 36.4 MPa), respectively. The concrete compressive strengths were determined using 4×8 in. (102×204 mm) concrete cylinders cast for each bridge deck and cured under the same conditions as the deck. Concrete was provided by a local ready-mix supplier.

Tension coupons of MMFX and Grade 60 steel were tested according to ASTM-A370 specifications. The measured stress-strain characteristics of the MMFX and grade 60 steel are shown in Figure 2. The MMFX reinforcing bars exhibit a linear stress-strain relationship up to 100 ksi (689 MPa) followed by a non-linear behavior with ultimate strength of 173 ksi (1193 MPa). According
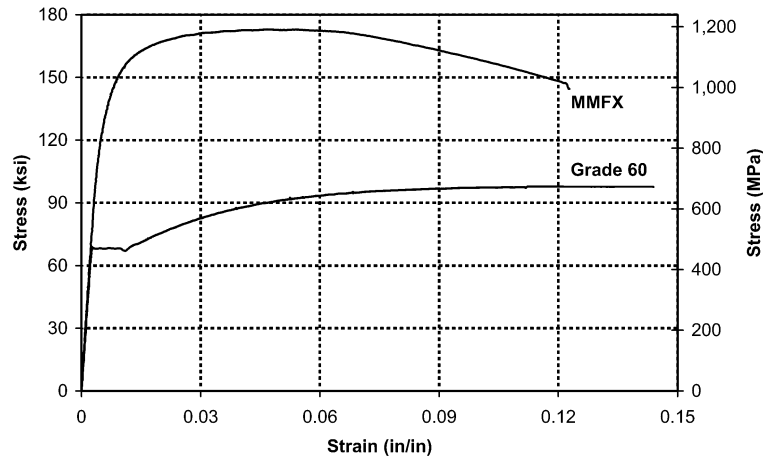
Fig. 2. Stress-strain characteristics of Grade 60 and MMFX steel.

to the ASTM-A370 offset method (0.2% offset) the yield strength of MMFX steel was found to be 120 ksi (827 MPa). The initial modulus of elasticity was determined to be 29,000 ksi (200 GPa), followed by a non-linear behavior and reduction in the modulus of elasticity at stress higher than 100 ksi (689 MPa). The yield strength of the Grade 60 steel was determined to be 68 ksi (469 MPa).

Test Setup and Instrumentation

Two 440 kips (1957 KN) MTS hydraulic actuators were used to apply a concentrated load to each span simultaneously to simulate the effect of a truck wheel load. Two 10×20 in. (254×508 mm) steel plates were used to transfer the load from the actuator to comply with the AASHTO LRFD Bridge Design Specifications for tire contact area. A 1/2 in. (13 mm) thick neoprene pad was placed under each loading plate to prevent possible local crushing of the concrete. The supporting girders were supported by concrete blocks to transfer the applied load to the strong floor resulting in a clear span of 96 in. (2438 mm). The clear span of supporting girders was determined based on the equivalency of the torsional stiffness of the supporting girders to that of the steel girders used in the actual bridge. Figure 3 shows an isometric view of the test setup and the first bridge deck prior to testing.

A total of 72 channels were used for instrumentation of each bridge deck. A 440 kips (1957 KN) load cell was mounted to each actuator to measure the applied load. Twenty-four string potentiometers (string pots) were used to measure the bridge deck deflection profiles along the longitudinal and transverse directions. In addition, six linear potentiometers were used to measure the girders deflections and rotations. Twenty PI gages were used to measure the concrete strain at various locations. The measured strains were used to determine the strain profiles of the sections at the measured locations. Twenty electrical resistance strain gages of 120 ohm and 6 mm gage length were attached to selected reinforcing bars to determine the strains in these bars. Data were electronically recorded by an Optim Megadac data acquisition system. Figure 4 shows the locations of the PI gages used and establishes the notation adopted hereafter.
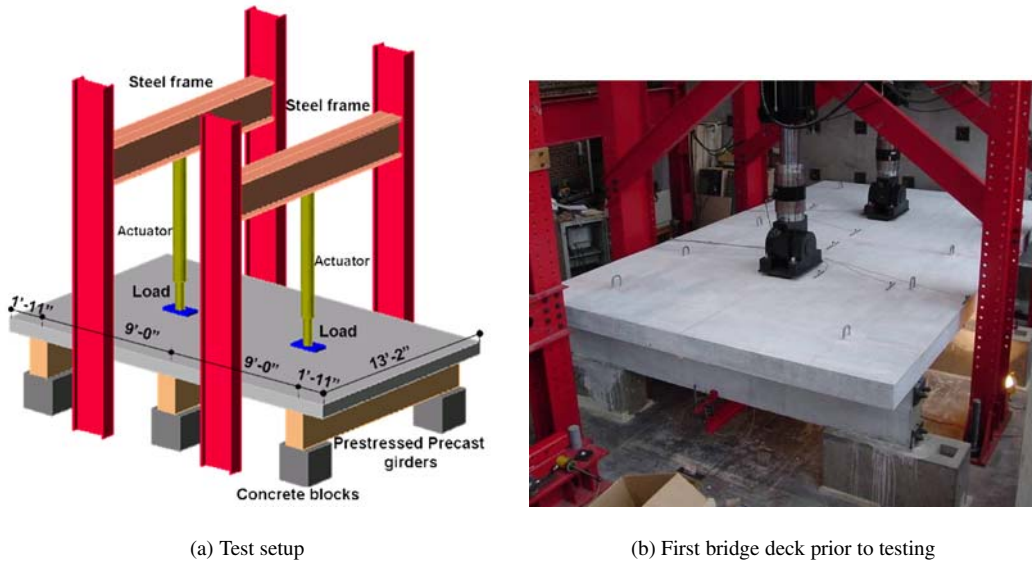
(a) Test setup

(b) First bridge deck prior to testing

Fig. 3. Test setup and the first bridge deck prior to testing.

(a) Location of PI gages
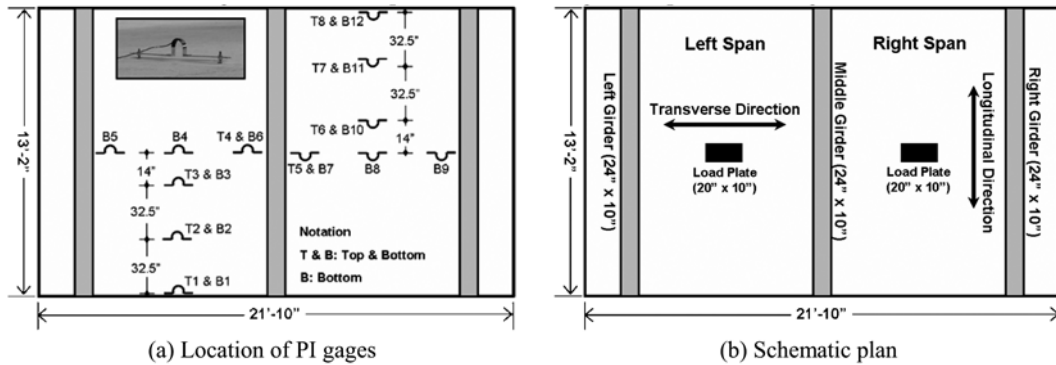
(b) Schematic plan

Fig. 4. PI gages locations and notations for the three bridge decks.

Experimental Results

Load-Deflection Behavior

The load-deflection envelopes up to failure for three bridge decks are given in Figure 5. It should be noted that deflection plotted in Figure 5 is measured at the center of the respective deck span directly under the applied load. It is readily apparent from Figure 5 that the first bridge deck reinforced with MMFX steel using the same reinforcement ratio as used for the actual bridge exhibited smaller deflection in comparison to the other two bridge decks. Due to the use of higher reinforcement ratio in the first bridge deck, stiffness was higher than the other two decks; this could also be due to the higher compressive strength of the concrete used for the first deck. Despite the lower reinforcement ratio used for the third bridge deck (33% less than the first two decks), it was capable of sustaining the same load as the second bridge deck of the Grade 60 steel. This behavior is attributed to the utilization of the higher tensile strength of MMFX steel. The slight increase of the deflection measured
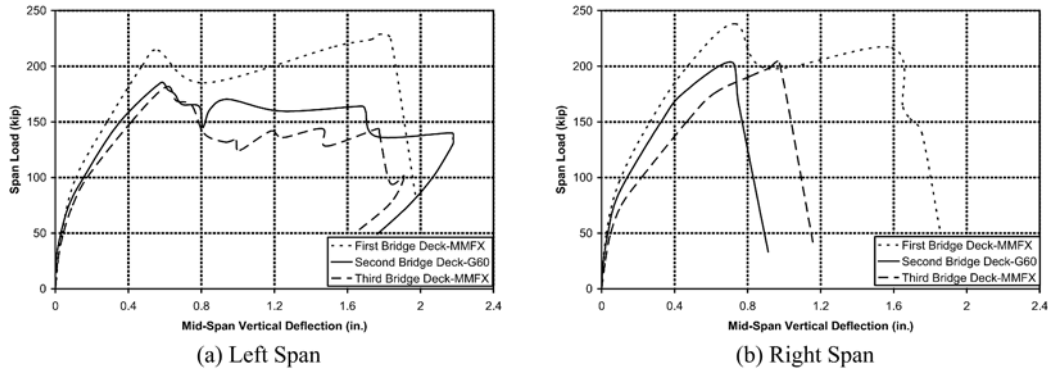
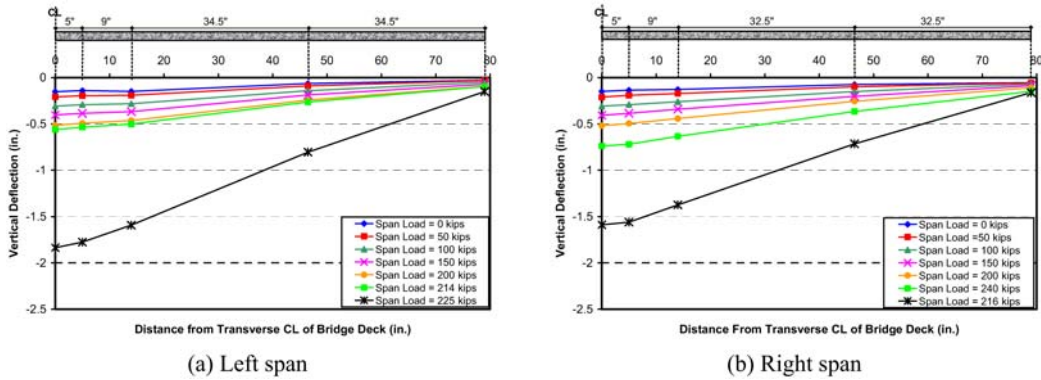**Fig. 5.** Load-Deflection envelope of the three bridge decks.

Fig. 6. Longitudinal deflection profile for the first bridge deck.

for the third bridge deck in comparison to the second deck is possibly due to the slight reduction of the modulus of elasticity of MMFX steel at high stress levels. According to the AASHTO LRFD Bridge Design Specifications (1998), the design tandem consists of a pair of 25 kips (111 KN) axles. Therefore, at a load level of 25 kips (111 KN), which is less than the cracking load; the deflection at service load was almost identical for the three bridge decks.

Deflection Profile

The deflection profiles along the longitudinal direction of the three bridge decks are given in Figures 6, 7, and 8, respectively. It should be noted that the deflection profiles are plotted for the final loading cycle only. The deflections shown for each deck represent the residual deflection from previous loading. The deflection profiles for the three bridge decks indicate that the deflection at the edge of the bridge decks was very small. This implies that selection of the length of the model is effective for carrying the total load, and therefore, representative to the actual bridge deck.

The deflection profiles along the transverse direction of the three bridge decks are given in Figures 9, 10, and 11, respectively. It should again be noted that the deflection profiles are plotted for the last loading cycle only, therefore residual deflections are shown at the beginning of the loading cycle (zero load). The deflection profiles indicate that the maximum deflection occurred at the mid-span under the applied load. Also, it is clear that the spans failed in punching shear (right span) exhibited less deflection than the spans failed due to flexural as will be discussed in the following sections.
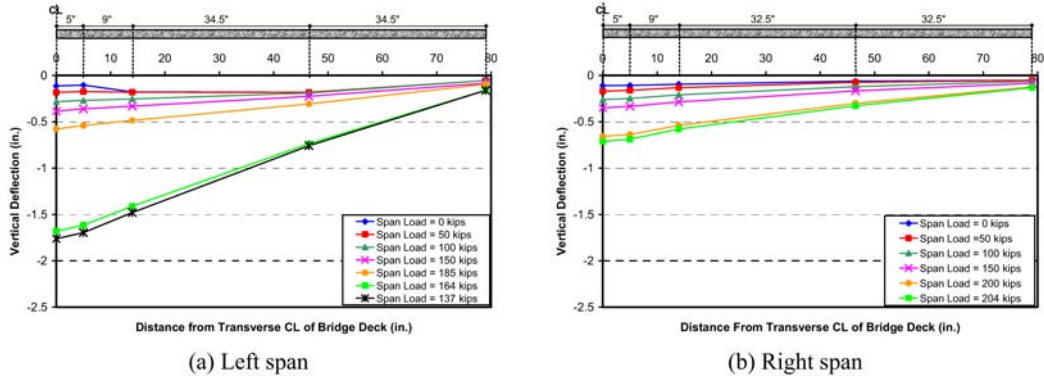
Fig. 7. Longitudinal deflection profile for the second bridge deck.
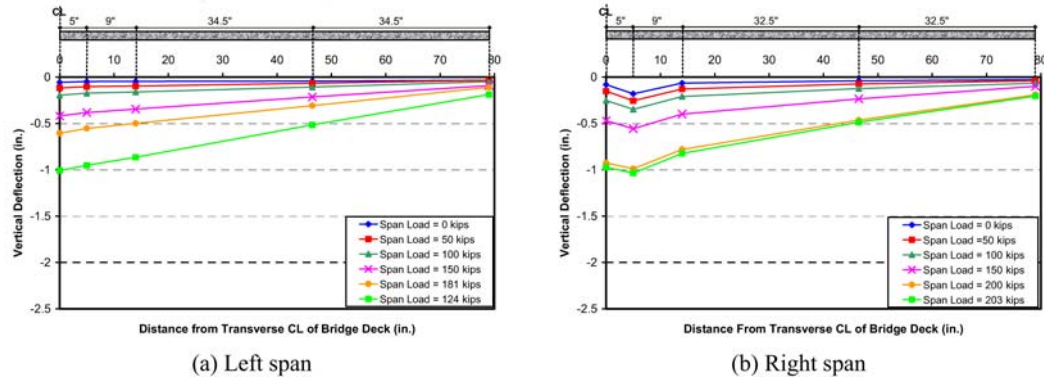

Fig. 8. Longitudinal deflection profile for the third bridge deck.

MODE OF FAILURE

In general, the behavior was two-way flexural mode followed by development of an arching action supported by membrane forces developed in the bottom layer of the reinforcement. At first peak load of the first bridge deck a sudden drop in the load occurred due to the formation of flexural-shear
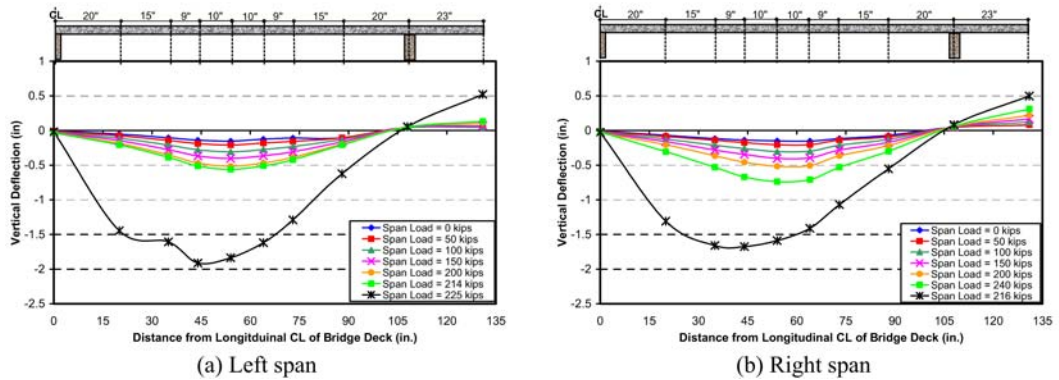

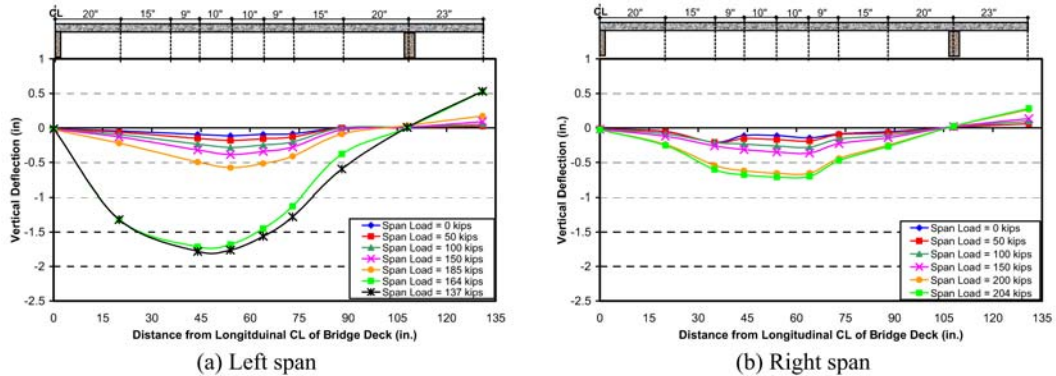Fig. 9. Transverse deflection profile for the first bridge deck.

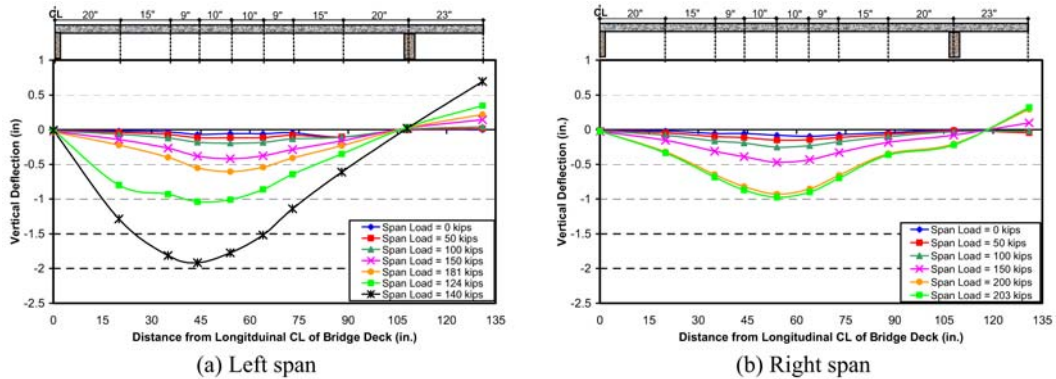**Fig. 10.** Transverse deflection profile for the second bridge deck.

Fig. 11. Transverse deflection profile for the second bridge deck.

cracks along the top surface of the bridge deck on both sides of the middle girder. Further loading led to the widening of those cracks associated with slight increase in the load resistance until punching failure occurred. Punching failure of both spans occurred simultaneously at a load level of 229 kips (1019 N) and 216 kips (961 N) for the left and right spans, respectively. Figure 12 shows the first bridge deck at the conclusion of the test, where the punching areas under the two loads and the shear cone at the bottom of the left span can be seen clearly.

The behavior of the second bridge deck, reinforced with grade 60 steel using the same reinforcement ratio was similar to the first deck. At the peak load of the left span, a sudden drop in the load occurred due to the formation of a flexural-shear crack on the top surface of the bridge deck to the left of the middle girder only (left span only). This drop in the load made the left span incapable to carry higher load equivalent to the punching shear capacity of the deck. The test was terminated due to excessive deflections in the left span. The smooth decrease of the load carrying capacity of the left span reveals that flexural-shear failure was the mode of failure of the left span. The maximum measured load for the left span was 185 kips (823 KN) and a deflection of 2.2 in. (56 mm) prior to termination. Failure of the right span was due to punching shear at a load level of 204 kips (907 KN).

Similar to the second bridge deck the right span of the third deck failed by punching shear prior to the failure of the left span. A flexural-shear crack formed in the left span causing a sudden drop in the load which made the left span incapable to carry more load equivalent to its punching shear resistance. Flexural-shear failure was the mode of failure of the left span as revealed by the smooth
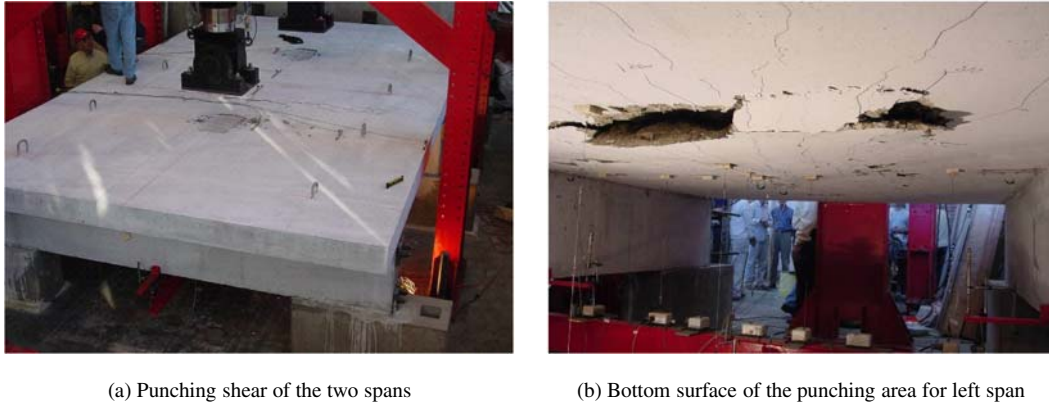
(a) Punching shear of the two spans   (b) Bottom surface of the punching area for left span

Fig. 12. Failure of the first bridge deck.

(a) Second bridge deck   (b) Third bridge deck
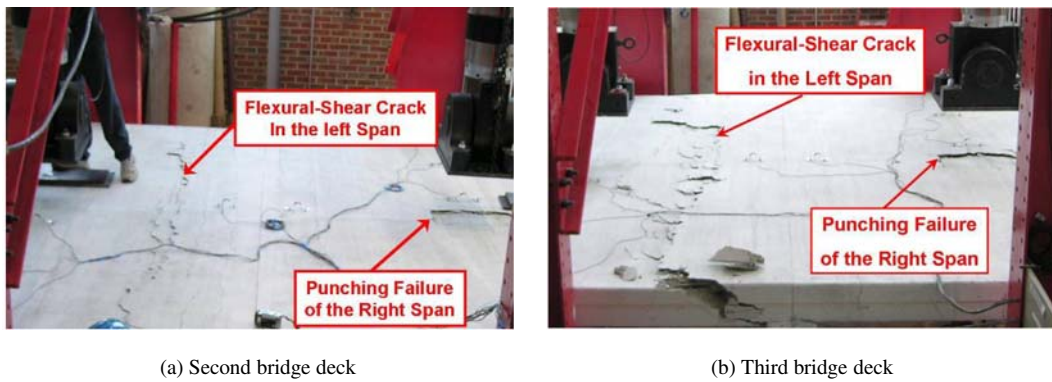
Fig. 13. Second and third bridge decks at failure.

decrease in the load carrying capacity of the load, whereas the right span failed in punching shear at a load level of 203 kips. The test terminated due to excessive deflections in the left span and the maximum recorded load for the left span was 181 kips (805 KN). Figure 13 shows the second and third bridge decks at failure, where the punching area under the actuator in the right span and the flexural-shear crack formed in the left span are clearly visible.

Crack Pattern

No cracks were observed up to a load level of 50 kips (222 KN) for any of the three bridge decks. However visible top cracks started to occur at a load level of roughly 60 kips (444 KN) for each deck. Figure 14 shows the top cracks at a load level of 100 kips. Negative flexural cracks formed before the positive cracks due to the higher values of negative moments in comparison to the positive moments.

Positive moment flexural cracks at load levels of 100 and 150 kips (444 and 666 KN) for the first bridge deck are shown in Figure 15, where the crack pattern confirms the two way distribution of the load. Further loading led to spreading and widening of the flexural cracks until the formation of the flexural-shear crack at the top surface of the deck close to the middle girder. The formation of the flexural-shear crack led to a sudden drop in the load as previously discussed. However, the flexural-shear crack formed symmetrically on both sides of the middle girder of the first bridge
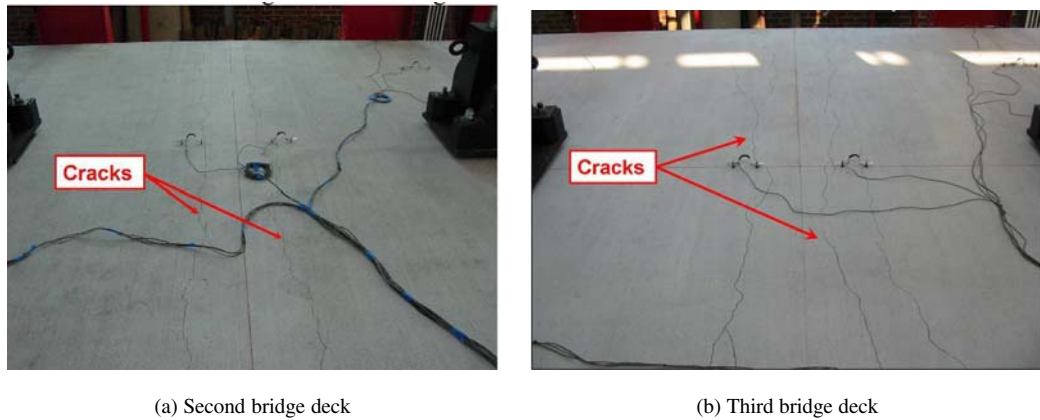
(a) Second bridge deck

(b) Third bridge deck

Fig. 14. Negative flexural cracks at load level of 100 kips for the second and third bridge decks.

(a) At load level of 100 kips
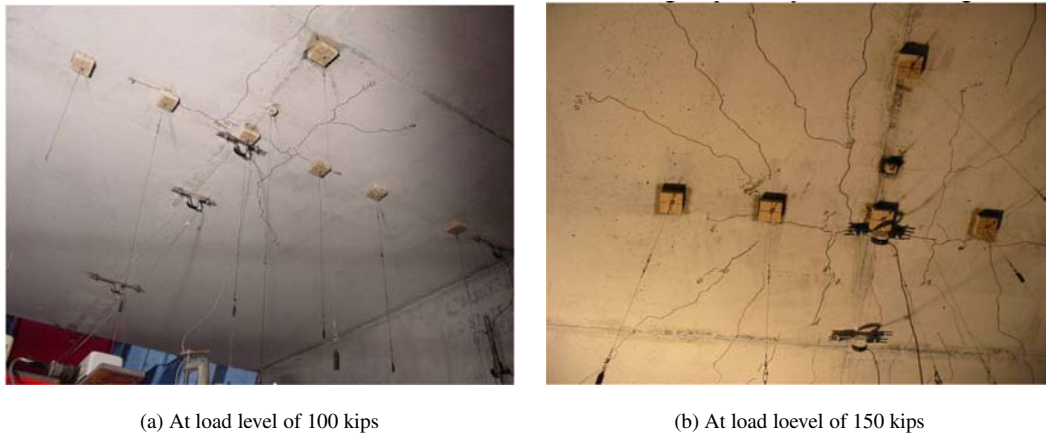
(b) At load loevel of 150 kips

Fig. 15. Positive flexural cracks for the first bridge deck.

deck, therefore allowed increase of the load to cause punching shear of both spans. For the second and third bridge decks, the flexural-shear crack occurred on the left side of the middle girder only which allowed the load to increase in the right span causing punching shear at the right span only as shown in Figure 13.

Strain Profiles and Girders Rotation

Based on the deformations measured by the PI gages, strain profiles were determined using the measured strain at the extreme top and bottom fibers of each bridge deck. It should be noted that all the strain profiles are plotted for the final loading cycle only, and therefore residual strains are shown at zero load. The strain profile obtained from the two PI gages located in the right span at 14 in. (356 mm) from the centerline of the deck (T6 and B10 in Figure 4) is depicted in Figure 16. The strain profile indicates that the top surface of the concrete at the vicinity of the punching area exceeded the limiting compressive strain value. The limiting compressive strain at a distance y from the edge of the loading plate reported by Kinnunen and Nylander (1960) was 0.0019, Marzouk and Hussein (1991) was 0.00215, and Mufti and Newhook (1998) was 0.002, where y is the distance from the bottom surface of the slab to the root of the shear crack at failure. The strain profile obtained from
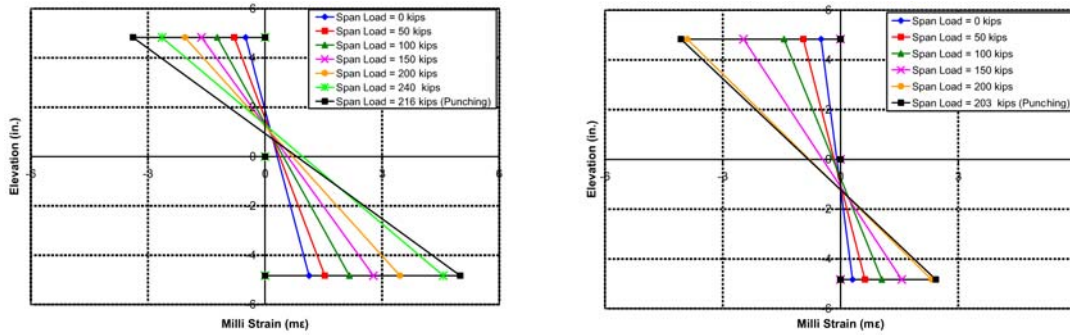
Fig. 16. Strain profile from T6 and B10 PI gages for the first and third bridge decks.

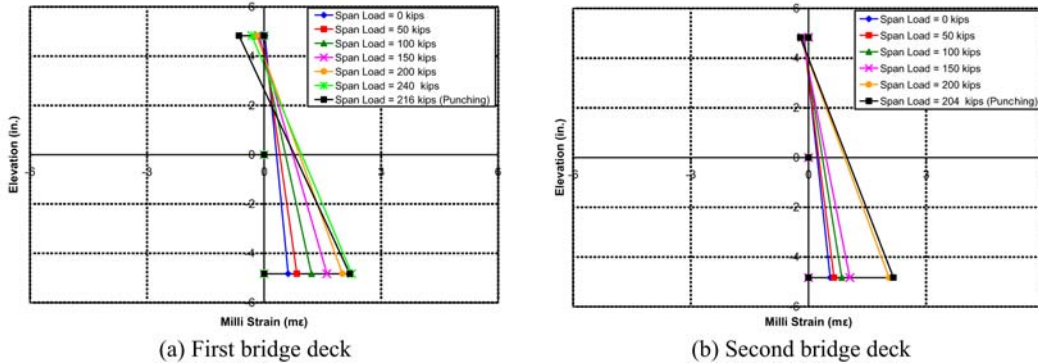(a) First bridge deck (b) Second bridge deck

Fig. 17. Strain profile from T8 and B12 PI gages for the three bridge decks.

the PI gages at the edge of the right span (T8 and B12 in Figure 4) is shown in Figure 17. The strain profile shows that the strain values were very small, which is another indication that the length of the bridge deck is effective and representative to the behavior of typical bridges.

Rotation of the three supporting girders was monitored throughout the test of the three bridge decks as shown in Figure 18. For all three decks the two outside girders exhibited larger rotations in comparison to the middle girder due to the unbalanced moment effect
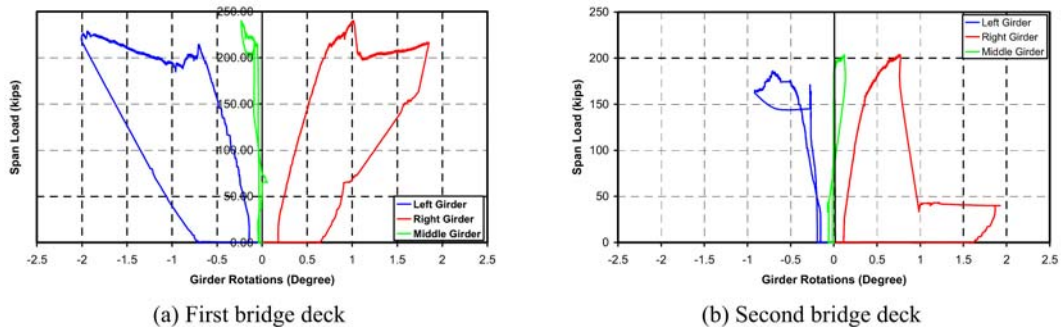

(a) First bridge deck (b) Second bridge deck

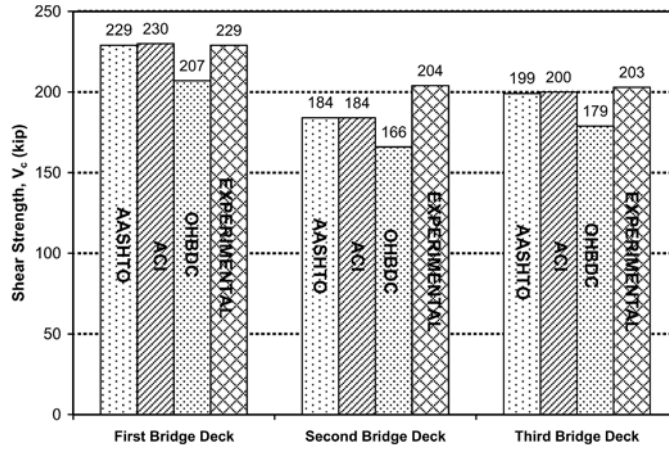**Fig. 18.** Rotation of supporting girders.

Fig. 19. Predicted and experimental shear strength of bridge decks.

Predicted Strength

The predicted shear strengths for the three bridge decks according to the different design codes are given in Figure 19 as well as the experimental values. The design codes included are: American Association of State Highway and Transportation Officials (AASHTO), American Concrete Institute (ACI 318-02), and Ontario Highway Bridge Design Code (OBBDC, 1991). The equations used are as follows:

$$\text{AASHTO:} \quad V_c = \min\left[0.063 + \frac{0.126}{\beta_c}; 0.126\right]\sqrt{f_c'}\, b_0 d; \text{ units: kips \& in.} \tag{1}$$

$$\text{ACI:} \quad V_c = \min\left[2 + \frac{4}{\beta_c}; 4; \frac{\alpha_s d}{b_0} + 2\right]\sqrt{f_c'}\, b_0 d; \text{ units: lbs \& in.} \tag{2}$$

$$\text{OHBDC:} \quad V_c = [0.6 f_r + 0.25 f_{pc}]b_0 d + 0.9 V_p; \text{ units: N \& mm,} \tag{3}$$

where V_c = punching shear capacity of bridge deck; β_c = ratio of long side to short side of loading plate; f_c' = concrete compressive strength; b_0 = perimeter of critical section at a distance of $d/2$ from loading plate; d = effective section depth; α_s = constant; f_r = concrete tensile strength; f_{pc} = compressive stress in concrete due to prestressing; and V_p = component of effective prestressing force in direction of applied shear.

It is clearly seen from Figure 19 that the predicted values according to the AASHTO and ACI design codes predict very well the measured values for the bridge decks using MMFX and Grade 60 steel.

Analytical Modeling

General

The three bridge decks were modeled using the finite element analysis program ?ANACAP? (Anatech Concrete Analysis Program) Version 3.0, (James, 2004). The concrete material model is based on smeared cracking methodology developed by Y. R. Rashid, 1960. Within the concrete constitutive
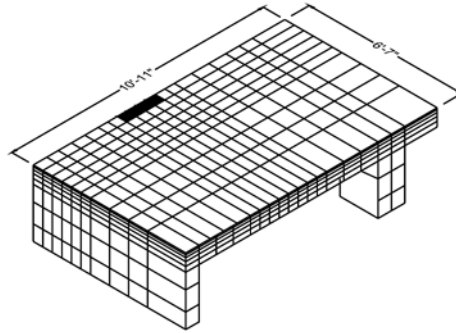
Fig. 20. Mesh used for modeling the three bridge decks.

model, cracking and all other forms of material non-linearity are treated at the finite element integration points. Cracks are assumed to form perpendicular to the principal tensile strain direction in which the criterion is exceeded and they are allowed to from at each material point. When cracking occurs, the normal stress across the crack is reduced to zero and distribution of cracks around the crack is recalculated. Cracks may close or re-open under load reversals. Concrete modeling also included residual tension stiffness for the gradual transfer of load to the reinforcement during crack formation. In addition, the program accounts for the reduction in shear stiffness due to cracking and further decay as the crack opens. The reinforcement is modeled as individual sub-elements within the concrete elements. The stiffness of the bar sub-element is superimposed on the concrete element stiffness in which the bar resides. The anchorage loss is modeled as an effective stiffness degradation of the bar as a function of the concrete strain normal to the bar.

A 3-D analysis was conducted for the three bridge decks using 20-node hexahedral continuum elements. Only one quarter of the deck was modeled due to its symmetry about both axes. The depth of the deck was divided into five layers within its thickness with a total number of elements of 1040, as shown in Figure 20.

Analytical Results

The predicted and experimental load-deflection envelopes for the three bridge decks are compared as shown in Figure 21. It can be seen that the predicted load-deflection behaviors of the three bridge decks compared very well with the measured values. The initial and post-cracking stiffnesses were very accurately predicted by the analytical model. In addition, the ultimate load was very reasonably predicted considering the fact the two spans of the second and third bridge decks failed in two different modes. However, the predicted ultimate deflection was slightly less than the experimental values; this is due to the nature of the smeared cracking methodology adopted by the program. For validation purposes the contours of the principal strain at failure and the portion of the first bridge deck that failed due to punching failure are shown in Figure 22. The strain contours depict the punching shear cone developed which matches very well the experimental failure shear cone.

Conclusions

1. The ultimate load carrying capacity of the three bridge decks tested in this investigation was eight to ten times the service load specified by AASHTO Design Specifications (1998).
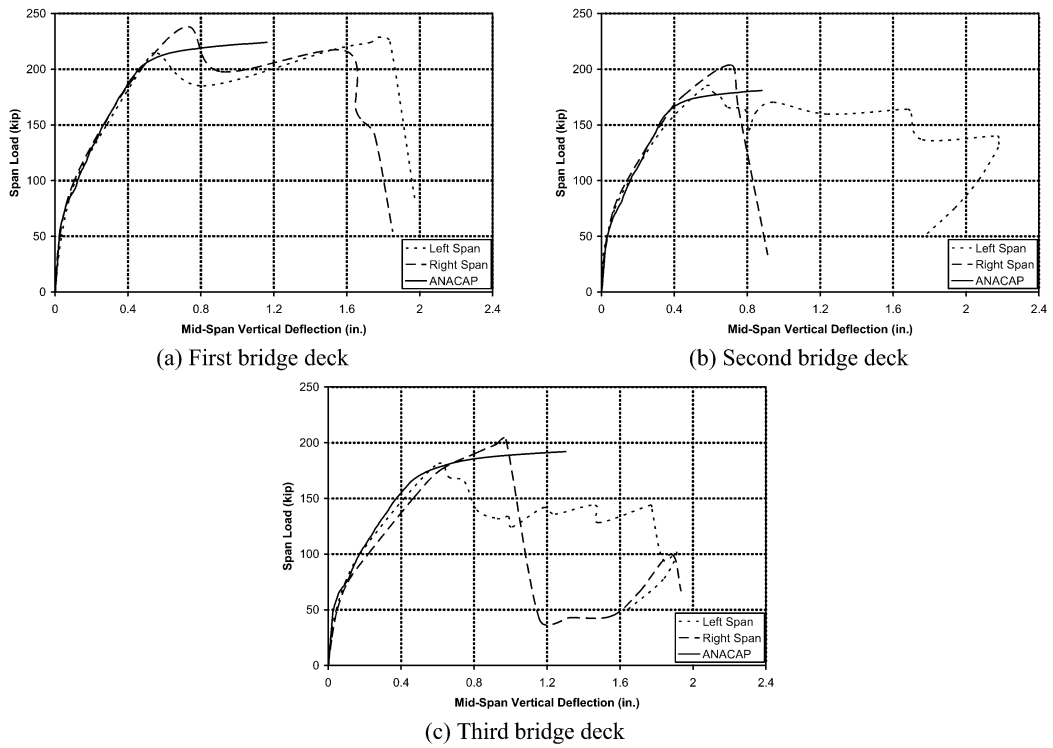2. Punching shear failure was the primary mode of failure for the three bridge decks tested.

(a) First bridge deck

(b) Second bridge deck

(c) Third bridge deck

Fig. 21. Analytical and experimental load-deflection envelopes for the three bridge decks.

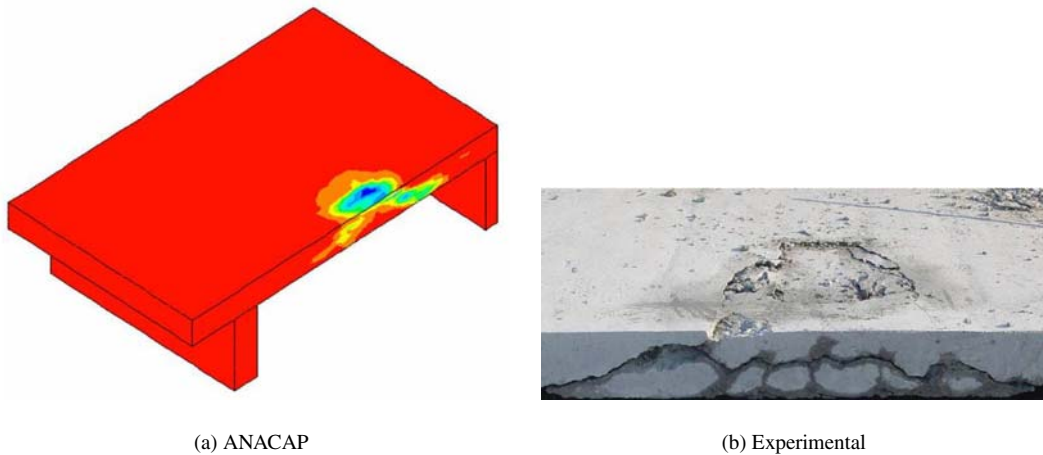
(a) ANACAP

(b) Experimental

Fig. 22. Principal strains contours at failure for the first bridge deck.

3. Punching failure resulted in sudden decrease of the load carrying capacity, while flexural failure resulted in gradual decrease of the load carrying capacity.
4. Bridge decks reinforced with MMFX steel exhibited same deflection at service load but developed more load carrying capacity when compared to decks reinforced with Grade 60 steel with the same reinforcement ratio.
5. Bridge decks reinforced with 33% less MMFX steel developed the same ultimate load carrying capacity and deflection at service load as those reinforced with Grade 60 steel. This is attributed to the higher strength of the MMFX steel compared to Grade 60 steel.

References

American Association of State Highway and Transportation Officials, 1998, ? "AASHTO LRFD Bridge Design Specifications", Washington, D.C.

American Concrete Institute (ACI), 2002, "Building Code Requirements for Structural Concrete", ACI 318-02, Farmington Hills, Michigan.

James, R.G., 2004, "ANACAP Concrete Analysis Program Theory Manual", Version 3.0, Anatech Corporation, San Diego, CA, 2004.

Kinnunen, S. and Nylander, H., 1960, "Punching of Concrete Slabs without Shear Reinforcement", *Transactions of the Royal Institute of Stockholm*, Sweden, No. 158.

Marzouk, H. and Hussein, A., 1991, "Punching Shear Analysis of Reinforced High-Strength concrete Slabs", *Canadian Journal of Civil Engineering*, 18, 954–963.

Mufti A.A. and Newhook, J.P., 1998, "Punching Shear Strength of Restrained Concrete Bridge Deck Slabs", *ACI Structural Journal*, 95(4), July–August, 375–381.

OHBDC, 1991, "Ontario Highway Bridge Design Code", Ministry of Transportation of Ontario, Downsview, Ontario

Rashid, Y.R., 1960, "Ultimate Strength Analysis of Prestressed Concrete Pressure Vessels", *Nucl. Eng. & Design*, pp. 334–344.